




A protein corona modulates the function of mineralization-competent matrix vesicles

Juçara Gastaldi Cominal¹ , Heitor Gobbi Sebinelli¹ , Larwsk Hayann¹ ,
Lucas Fabrício Bahia Nogueira¹ , Marcos Antonio Eufrásio Cruz¹ , Maryanne Trafanni Mello¹ ,
Luiz Henrique da Silva Andrioli^{1,2} , Maytê Bolean¹ , Ana Paula Ramos¹ , Saida Mebarek³ ,
Massimo Bottini^{2,4,*} , José Luis Millán^{2,*} , Pietro Ciancaglini^{1,*} 

¹Departamento de Química, Faculdade de Filosofia, Ciências e Letras de Ribeirão Preto, Universidade de São Paulo, Ribeirão Preto 14040-901, Brazil

²Sanford Children's Health Research Center, Sanford Burnham Prebys Medical Discovery Institute, La Jolla, CA 92037, United States

³Institut de Chimie et Biochimie Moléculaires et Supramoléculaires, UMR CNRS 5246, Université Claude Bernard Lyon 1, 69 622 Villeurbanne Cedex, France

⁴Department of Experimental Medicine, University of Rome Tor Vergata, 00133 Rome, Italy

*Corresponding authors: Massimo Bottini, Department of Experimental Medicine, University of Rome Tor Vergata, 00133 Rome, Italy (massimo.bottini@uniroma2.it); José Luis Millán, Sanford Children's Health Research Center, Sanford Burnham Prebys Medical Discovery Institute, La Jolla, CA 92037, United States (millan@sbpdiscovery.org); and Pietro Ciancaglini, Departamento de Química, Faculdade de Filosofia, Ciências e Letras de Ribeirão Preto, Universidade de São Paulo, Ribeirão Preto 14040-901, Brazil (pietro@ffclrp.usp.br).

Abstract

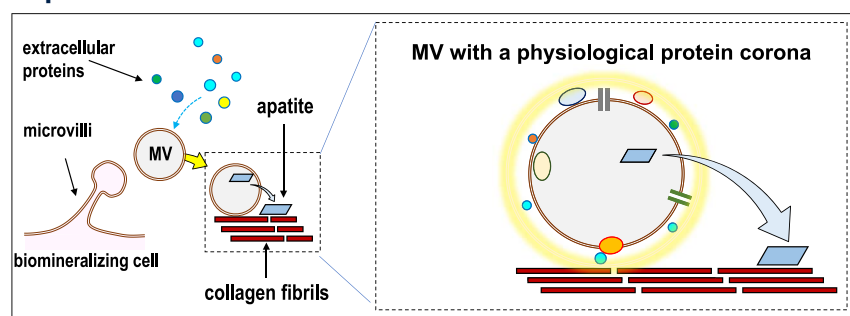
Mineralizing cells release a special class of extracellular vesicles known as matrix vesicles (MV), crucial for bone mineralization. Following their release, MV anchor to the extracellular matrix (ECM), where their highly specialized enzymatic machinery facilitates the formation of seed mineral within the MV's lumen, subsequently releasing it onto the ECM. However, how MV propagate mineral onto the collagenous ECM remains unclear. In this study, we address these questions by exploring the "protein corona" paradigm whereby nanoparticles entering a biological milieu become cloaked by a corona of soluble proteins modifying their biological functions. We isolated native MV from the growth plates of chicken embryos. After removing the protein corona from the native MV using high ionic strength buffer, we obtained shaved MV. Reconstituted MVs were produced by incubating shaved MV with the removed protein corona constituents. Our results show that both the removal and reconstitution of protein corona significantly affect the biochemical and physicochemical properties of MV, resulting in 3 well-defined groups. Shaved MV exhibited an increase in tissue nonspecific alkaline phosphatase (TNAP) activity and a decrease in mineral deposition compared to native MV. Reconstituted MV partially recovered these functions, showing a reduction of TNAP activity and mineral deposition compared to native MV. Furthermore, changes in the protein corona affect the MV ability to anchor to the collagenous ECM, which is crucial for initiating the propagation of the mineral phase within this organic matrix. Proteomic analyses revealed changes in the protein profile of the MV resulting from the removal of the protein corona, indicating that shaved proteins were primarily related to external structural and ECM organization and catabolism. These findings underscore the role of the protein corona in modulating the mineralization capabilities of MV. Understanding these interactions could lead to new therapeutic strategies for enhancing bone repair and regeneration.

Keywords: protein corona, matrix vesicle, biomineralization, collagen scaffold, mineral nucleation, mineral propagation, hydroxyapatite

Lay Summary

Mineralization-competent cells produce matrix vesicles (MV) that work as nanoreactors in the initiation of bone mineralization. Once released to the extracellular space, MV interact with molecules present in the biological fluids, adsorbing them onto the vesicles' surface to form a "protein corona" that can modulate the biological functions of MV. Here we show that the removal of the protein corona affects collagen binding and the enzymatic activity of a crucial MV enzyme, while reconstitution of the protein corona reverses those deficits. Our findings provide novel valuable insights for the development of biomimetic materials for bone regeneration medicine applications.

Graphical Abstract



Received: September 12, 2024. Revised: December 3, 2024. Accepted: December 19, 2024

© The Author(s) 2024. Published by Oxford University Press on behalf of The American Society for Bone and Mineral Research.

This is an Open Access article distributed under the terms of the Creative Commons Attribution Non-Commercial License (<https://creativecommons.org/licenses/by-nc/4.0/>), which permits non-commercial re-use, distribution, and reproduction in any medium, provided the original work is properly cited. For commercial re-use, please contact journals.permissions@oup.com

Introduction

Bone formation is an orchestrated process involving mineralization-competent cells, such as mature osteoblasts and hypertrophic chondrocytes, which regulate the synthesis of the organic components of the extracellular matrix (ECM), including its main constituent, collagen, as well as the deposition of hydroxyapatite (HAp) on the collagenous matrix. Mineralization-competent cells are enriched in Ca^{2+} and inorganic phosphate (P_i) transporters to maintain appropriate levels of these precursors of the mineral phase, in balance with mineralization inhibitors while ensuring an adequate protein framework in the ECM.¹ The prevailing theory describes that biomineralization commences within a compartmentalized environment of a specific class of extracellular vesicles (EV) referred to as matrix vesicles (MV). MV have diameters ranging from 100 to 300 nm and their biogenesis is still not completely elucidated, but it is widely assumed that they form by budding from the microvilli of mature osteoblasts and hypertrophic chondrocytes.^{2–5} The formation of a nucleation core, and maturation of seed mineral are considered key functions of MV, and are strongly supported by: (1) the presence of a precursor seed of the minerals in the MV's lumen, made of amorphous aggregates of Ca^{2+} and P_i complexed with phospholipids, such as phosphatidylserine and annexins;^{2,6–8} and (2) the cartilaginous bone matrix presents minerals associated with lipids corresponding to those present in the vesicles.^{1,6} Additionally, MV have a unique enzymatic machinery, including PHOSPHO1 and the tissue nonspecific alkaline phosphatase (TNAP) that generate P_i intravesicularly and perivesicularly, respectively.^{9,10}

It is important to note that mineralization-competent cells can also produce other types of EV, which can be purified from the supernatant of cell culture or biological fluids without the collagenase digestion.⁵ The state-of-the-art describes MV as the only class of EV capable of anchoring to the collagen-rich bone ECM propagating mineralization but how this is accomplished is not clearly understood.^{11,12}

Recently, a new paradigm suggested that once MV are released in the extracellular milieu, soluble proteins and biological factors present in the microenvironment can adsorb onto the vesicles' surface and form a "protein corona" that can modulate the biological functions of these vesicles.¹³ Protein corona formation phenomena and its biological effects have been extensively described for synthetic nanoparticles¹⁴ and for other classes of EV different from MV.^{13,15–18} Depending on the protein corona composition, the biomolecules adsorbed to/acquired by the EV surface can promote changes in their physicochemical properties, stimulate or decrease cellular interactions, and affect targeted delivery and biodistribution. Therefore, the protein corona has the potential to modulate the function of EV in several processes, including immune responses, coagulation, infections, diseases, and biomineralization.^{13,19,20}

In the present study, we identify the composition of the protein corona present on the surface of MV released by chondrocytes isolated from the epiphyses/growth plates of chicken embryos. We focused on their biological identity and function, particularly in relation to bone mineralization, which includes the enzymatic machinery, the anchoring specificity of MV to a collagen-based matrix, and ability to propagate mineral.

Materials and methods

Native MV isolation from chicken embryo femurs

MV were prepared with a necessary collagenase digestion step⁴ following the MISEV2023 recommendations.²¹ Briefly, chicken embryos were sacrificed 17 d after fertilization. Identification of the sex of each chicken embryo was not possible visually, but the egg supplier estimated that ~60–70% of the eggs resulted in male embryos. Femurs were dissected, the epiphyses/growth plates were finely cut into slices (1–3 mm thick), and digested for 3 hr at 37 °C in synthetic cartilage lymph (SCL) buffer, pH 7.6, supplemented with 1 mmol L^{-1} CaCl_2 and with type I collagenase from *Clostridium histolyticum* (300 U per gram of dissected tissue). The SCL buffer is composed of 1.83 mmol L^{-1} NaHCO_3 , 12.7 mmol L^{-1} KCl, 0.57 mmol L^{-1} MgCl_2 , 5.55 mmol L^{-1} D-glucose, 63.5 mmol L^{-1} sucrose, 16.5 mmol L^{-1} Tris (2-Amino-2-hydroxymethyl-propane-1,3-diol), 100 mmol L^{-1} NaCl, 0.7 mmol L^{-1} Na_2SO_4 in water at pH 7.6.²² After digestion, the suspension was filtered through a 100 μm nylon membrane and centrifuged at $600 \times g$ for 15 min to remove cell debris. The pellet was discarded, and the supernatant was subjected to consecutive centrifugations: first at $20\,000 \times g$ for 30 min and followed by a second at $80\,000 \times g$ for 1 hr, both at 4 °C. The final pellet obtained, which corresponds to native MV, was homogenized in 400 μL of SCL buffer. All procedures involving the euthanasia of animal embryos were approved by the ethics committee of FFCLRP protocol 19.1.842.59.13. Figure 1A summarizes the workflow of MV isolation and purification.

Shaved and reconstituted MV

Isolated native MV (200 μL) were incubated with 200 μL of SCL buffer, pH 7.6, containing 0.4 mol L^{-1} NaCl for 15 min, at 4 °C and ultracentrifuged for 1 hr at $80\,000 \times g$ at 4 °C. The removed supernatant solution containing the protein corona was dialyzed to remove all the NaCl salt. The shaved MV was obtained in the pellet and were rapidly washed and resuspended in 200 μL of SCL buffer, pH 7.6. The reconstitution process starts with the incubation of (100 μL) shaved MV with 300 μL of dialyzed protein corona, during 15 min at 4 °C. The mixture was ultracentrifuged for 1 hr, $100\,000 \times g$ at 4 °C, and the obtained pellet was carefully washed and resuspended in 200 μL SCL buffer, resulting in the reconstituted MV. All samples obtained in each step were flash frozen in liquid nitrogen and stored at –20 °C. Figure 1B summarizes the workflow of shaved and reconstituted MV obtention.

Vesicle characterization

The mean diameter, and zeta potential were determined using dynamic light scattering (DLS, Malvern). Vesicle concentration was determined by nanoparticle tracking analysis (NTA, NS3000, Malvern). Total protein content was determined as per Hartree method.²³ Morphological analysis by atomic force microscopy (AFM) used a SPM-9600 Scanning Probe Microscope (Shimadzu Co., Japan) in intermittent mode with silicon probes having a hardness ranging from 34 to 50 N m^{-1} and resonance frequency between 324 and 369 Hz. Samples were prepared on mica cleaved at time of use at a 5.0 % (w/v) glutaraldehyde.²⁴ TNAP activity was measured as before.⁴ SDS- and non-denaturing polyacrylamide gel were conducted as per established protocols using 15 μg of total protein

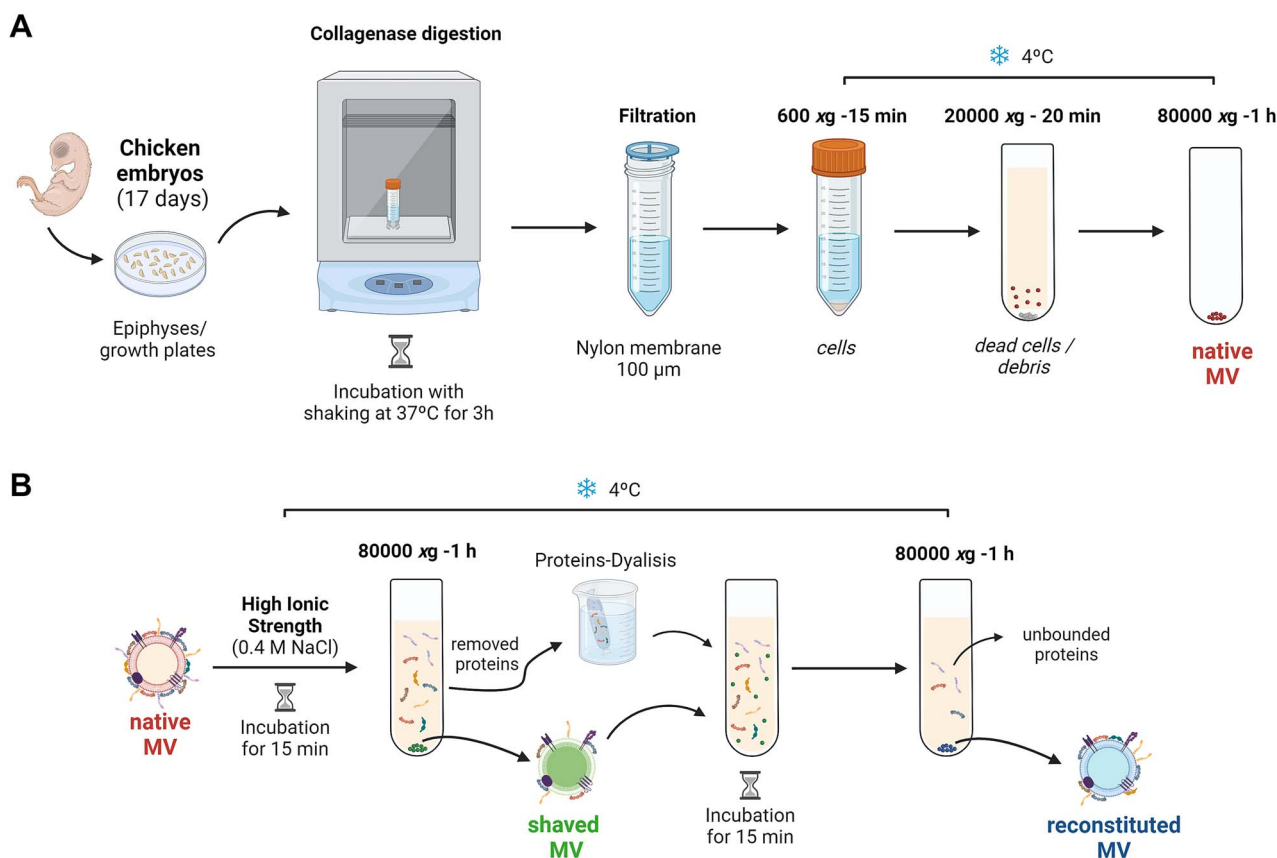


Figure 1. Schematic procedure for MV isolation. (A) Native MV isolation from growth plates of chicken embryos femurs. (B) Shaved MV and reconstituted MV methodology sequence. Procedures details were fully described in “Materials and Methods”. Created with [BioRender.com](#). Abbreviation: MV, matrix vesicle.

of each vesicle.²⁵ The phosphohydrolytic activity assay was carried out as before.²⁶

Mineralization assay

20 µg of total protein of each vesicle were incubated in 96 wells plates, for 22 hr at 37°C, in SCL buffer containing 2 mmol L⁻¹ CaCl₂ and 2.0 mmol L⁻¹ adenosine triphosphate (ATP) or Na₂HPO₄ (final volume adjusted to 200 µL). The turbidity was measured at 340 nm, with 5-min intervals, in triplicates.¹⁰ Curves of turbidity (Abs_{340 nm}) vs time (hr) were plotted, and the sigmoidal tendency of mineral formation was evaluated using a mathematical approach.²⁷ Mineralization-related parameters obtained were: initial mineralization time (t_i), which is characterized by a rapid increase in U; final mineralization time (t_f), which is characterized by a decrease in U; time in which the maximum rate of mineral formation is reached ($t_{max\ rate}$), corresponding to the peak of the dU/dt curve; the maximum of turbidity (U_{max}) at Abs_{340 nm}; and the potential of mineral propagation rate ($U_{max/tmax\ rate}$), which measures the tendency of mineral formation. After the mineralization assay, the 96-well plate was placed in desiccator with silica and allowed to dry for 1 wk. The produced mineral was analyzed by means of 3 independent Fourier-transform infrared (FTIR) spectroscopy readings (IRPrestige-21, Shimadzu Co., Japan) using a ZNSE crystal attenuated total reflectance accessory.

Preparation of collagen scaffold

Solution of Type I collagen isolated from the mice tails was concentrated to ~10 mg·mL⁻¹ and added into a cylindrical Teflon template. The template was then exposed to an NH_{3(g)}

atmosphere, in a sealed desiccator for 24 hr to promote in vitro fibrillogenesis. The resulting hydrogel was dehydrated in a climate chamber at 37°C with 40% humidity control. This protocol was developed by our group and the detailed procedure is reported in Nogueira et al.²⁸

Scanning electron microscopy

20 µg total protein of each vesicle were placed onto the scaffold at the bottom of a 96-well plate. SCL buffer, pH 7.6, containing 2.0 mmol L⁻¹ of CaCl₂ and 2.0 mmol L⁻¹ of ATP, was add (volume adjusted to 200 µL), and the plate incubated at 37°C. The buffer was removed from each well and all scaffolds underwent post-fixation in 4 wt.% paraformaldehyde for 30 min and 1 wt.% OsO₄ for 2 hr. Subsequently, they were rinsed and treated with thiocarbonylhydrazide, followed by ethanol dehydration and critical point-drying with liquid CO₂. The dried samples were then mounted on aluminum stubs, gold-coated, and analyzed using a Shimadzu SS-500 SEM microscope (Shimadzu Co., Japan). Morphological changes in collagen-based scaffolds were examined, before and after 48 hr incubation.

Proteomic analysis of vesicles

Sample preparation

10 µg of total protein of each vesicle were subjected to an in-solution tryptic digest using a modified version of the single-pot solid-phase-enhanced sample preparation (SP3) protocol.^{29,30} 1% (w/v) SDS-containing lysates were added to Sera-Mag Beads (Thermo Scientific, #4515-2105-050250, 6515-2105-050250) in 10 µL 15% (v/v) formic acid and 30 µL of ethanol. Protein binding was achieved by shaking for 15 min

at room temperature. SDS was removed by 4 subsequent washes with 200 μL of 70% (v/v) ethanol. Proteins were digested overnight, at room temperature, with 0.4 μg of sequencing-grade modified trypsin in 40 μL of Hepes/NaOH (pH 8.4) in the presence of 1.25 mmol L^{-1} TCEP and 5 mmol L^{-1} chloroacetamide. Beads were separated, washed with 10 μL of an aqueous 2% (v/v) dimethyl sulfoxide solution, and the combined eluates were dried down. Peptides were reconstituted in 10 μL of H_2O and reacted for 1 hr at room temperature with 80 μg of labeling reagent TMT10plex (Thermo Scientific, #90111), previously dissolved in 4 μL of acetonitrile.³¹

Excess TMT reagent was quenched by the addition of 4 μL of an aqueous 5% (w/v) hydroxylamine solution and a 15 min incubation. Each sample was transfer to a new microcentrifuge tube and speedvac to dried labeled peptide sample. Peptides were reconstituted in 0.1 % (v/v) formic acid, and equal volumes were mixed. Mixed peptides were purified by a reverse-phase clean-up step (OASIS HLB 96-well $\mu\text{Elution}$ Plate, Waters #186001828BA). Peptides were subjected to an off-line fractionation under high pH conditions,³⁰ yielding 6 fractions.

LC-MS/MS analysis

Peptides were separated using an Ultimate 3000 nano RSLC system (Dionex) equipped with a trapping cartridge (Precolumn C18 PepMap100, 5 mm, 300 μm i.d., 5 μm , 100 \AA) and an analytical column (Acclaim PepMap 100. 75 \times 50 cm C18, 3 mm, 100 \AA) connected to a nanospray-Flex ion source. The peptides were loaded onto the trap column at 30 $\mu\text{L min}^{-1}$ using solvent A (0.1% formic acid, v/v) and eluted using a gradient from 2% to 40% solvent B (0.1% formic acid in acetonitrile, v/v) over 2 hr at 0.3 $\mu\text{L min}^{-1}$ (all solvents were of LC-MS grade). The Orbitrap Fusion Lumos was operated in positive ion mode with a spray voltage of 2.4 kV and capillary temperature of 275°C. Full scan MS spectra with a mass range of 375-1500 m z^{-1} were acquired in profile mode using a resolution of 120,000 (maximum fill time of 50 ms or a maximum of 4×10^5 ions [AGC]) and an RF lens setting of 30%. Fragmentation was triggered for 3 s cycle time for peptide-like features with charge states of 2-7 on the MS scan (data-dependent acquisition). Precursors were isolated using the quadrupole with a window of 0.7 m z^{-1} and fragmented with a normalized collision energy of 38. Fragment mass spectra were acquired in profile mode with a resolution of 30,000. Maximum fill time was set to 64 ms or an AGC target of 1×10^5 ions. The dynamic exclusion was set to 45 s. Acquired data were analyzed using IsobarQuant³² and Mascot V2.4 (Matrix Science) using a reverse UniProt FASTA *Homo sapiens* database (UP000005640) including common contaminants. The following modifications were considered: Carbamidomethyl (C, fixed), TMT10plex (K, fixed), Acetyl (N-term, variable), Oxidation (M, variable), and TMT10plex (N-term, variable). The mass error tolerance for full scan MS spectra was set to 10 ppm and for MS/MS spectra to 0.02 Da. A maximum of 2 missed cleavages were allowed. A minimum of 2 unique peptides with a peptide length of at least 7 amino acids and a false discovery rate (FDR) below 0.01 were required on the peptide and protein level.³³

Data analysis

Acquired data were analyzed using FragPipe³⁴ and a *Gallus gallus* Uniprot fasta database (UP00000539, ID9031, 4371

entries, last modified January 1, 2023, downloaded March 27, 2023) including common contaminants. The following modifications were considered: Carbamidomethyl (C, fixed), TMT10plex (K, fixed), Acetyl (N-term, variable), Oxidation (M, variable), and TMT10plex (N-term, variable). The mass error tolerance for full scan MS spectra was set to 10 ppm and for MS/MS spectra to 0.02 Da. A maximum of 2 missed cleavages were allowed. A minimum of 2 unique peptides with a peptide length of at least 7 amino acids and an FDR below 0.01 were required on the peptide and protein level.³³ The raw output files of FragPipe [protein.tsv – files³⁴] were processed using the R programming language (ISBN 3-900051-07-0). Contaminants were filtered out, and only proteins that were quantified with at least 2 razor peptides were considered for the analysis. Log2 transformed raw TMT reporter ion intensities were first cleaned for batch effects using the “removeBatchEffects” function of the limma package³⁵ and further normalized using the variance stabilization normalization package.³⁶ Proteins were tested for differential expression using a moderated t-test by applying the limma package. The replicate information was added as a factor in the design matrix given as an argument to the “lmFit” function of limma. A protein was annotated as a hit if it has an FDR below 5% and a resulting fold-change of at least 100%. A candidate protein was defined as having an FDR below 20% and a resulting fold change of at least 50%. Proteins that did not meet these criteria were annotated as “no hit”.

Statistical analysis

The values were reported as mean \pm SD of the mean. Considering the results obtained from the physicochemical analyzes, the groups were compared by the 2-way ANOVA followed by Tukey’s test for all the datasets. Statistical significance was set at $p < .05$ unless otherwise stated, and results were graphically presented using bar graphs or scatter plots as appropriate.

Results

Biochemical and biophysical characterization of vesicles

In this first proof-of-concept study we chose to use chicken embryos as the source of chondrocyte-derived MV for 2 main reasons: (1) the extensive literature regarding the biogenesis and function of chicken MV already available^{1,4,5,7} and (2) to be able to probe the composition and function of the protein corona derived from biological fluids extracting the MV from whole articulations, rather than from cells in culture. We characterized the biochemical and biophysical properties of 3 groups of vesicles: (1) native MV; (2) vesicles obtained by shaving the protein corona off from the native MV’s surface (shaved MV); and (3) vesicles obtained by incubating shaved MV with the protein corona that had been shaved off (reconstituted MV) (Table 1, Figure 2).

The mean diameter of all vesicles, measured by DLS, ranged from 185 to 225 nm, with a polydispersity index of ~ 0.2 , indicating a relatively homogeneous population. The zeta potential increased from -9.6 to -5.7 mV once the protein corona was shaved off, then decreased to -18.9 mV after reconstitution of the protein corona (Table 1). NTA analysis revealed the size distribution between MV groups, with the prevalent size ($>65\%$) being between 150 and 300 nm (Figure 2A). This suggests differences in the composition of surface proteins between native and reconstituted MV.

Table 1. Biophysical and biochemical characteristics of native MV, shaved MV, and reconstituted MV. Native MV was used as a 100% that corresponds to 2.61 mg/mL of total protein and 4.24 U/mg of specific activity of TNAP.

MV	NTA particle/mL	Protein recovered (%)	Specific activity (%)	$\mu\text{g protein/particle} \times 10^{-9}$	DLS diameter (nm)	Zeta potential (mV)	AFM Diameter (nm)	Medium height (nm)	Ratio roughness (nm)
Native	$5.97 \pm 4.69 \times 10^{10}$	100	100	$4.37 \pm 3 \times 10^7$	185 ± 23	-9.6 ± 0.3	185 ± 20	4.47 ± 2.0	0.58 ± 0.03
Shaved	$5.32 \pm 4.66 \times 10^{10}$	67.1 ± 2.3	108.1 ± 10.2	$3.17 \pm 2 \times 10^7$	225 ± 21	-5.7 ± 0.2	105 ± 10	2.04 ± 1.05	0.73 ± 0.02
Reconstituted	$3.56 \pm 1.23 \times 10^{10}$	73.6 ± 4.9	50.5 ± 9.81	$3.29 \pm 5 \times 10^7$	197 ± 32	-18.9 ± 0.4	146 ± 77	9.04 ± 3.00	1.09 ± 0.02
Statistical analysis (p value)									
MV \times sMV	0.7235	-	0.0271*	<0.0001	0.2187	<0.0001	0.1665	0.4191	0.0006
MV \times rMV	0.0009	-	<0.0001*	<0.0001	0.8404	<0.0001	0.5857	0.0921	<0.0001
sMV \times rMV	0.0017	-	<0.0001*	0.0062	0.4309	<0.0001	0.5566	0.0180	<0.0001

Abbreviations: AFM, atomic force microscopy; DLS, dynamic light scattering; MV, matrix vesicle; NTA, nanoparticle tracking analysis; TNAP, tissue nonspecific alkaline phosphatase. Data are reported as mean \pm SD. Two-way ANOVA followed by Tukey's test was applied and p value < 0.05 was considered statistically significant (bold). *Statistical analysis of TNAP specific activity (U mg^{-1}), Figure 2D.

High ionic strength treatment removed $\sim 33\%$ of proteins from the MV's surface. Incubation of shaved MV with the removed protein corona led to an $\sim 7\%$ increase in the vesicles' protein content. Additionally, native MV showed the highest ratio of protein content per particle, while shaved MV had the lowest ratio (Table 1). SDS-PAGE revealed differences in the protein profiles among native MV, shaved MV, and reconstituted MV: (1) absence of bands between 100 to 130 kDa and 10 to 15 kDa; (2) a slight reduction in bands between 15 to 50 kDa (Figure 2B). Altogether, these results indicated the non-complete reversibility of the process of protein corona removal and reconstitution.

Of interest, shaved MV displayed an increase in TNAP activity (Table 1, Figure 2C-E), while reconstituted MV showed a decrease. These differences in TNAP activity between native, shaved, and reconstituted MV might be due to changes in steric hindrance of the active site or to specific interaction with protein corona components that modulate TNAP activity (Figure 2E).

The physical properties of vesicles were also evaluated by AFM (Table 1 and Figure 3). The diameter obtained from AFM topographic images was in the order of native MV > reconstituted MV > shaved MV, consistent with the protein recovery results. Interestingly, the mean diameter obtained from AFM topographic images for native MV and reconstituted MV was similar to that calculated by DLS, while in shaved MV, the mean diameter was approximately half. This result could be explained by a partial aggregation of shaved MV in solution due to the absence of the protein corona.

The AFM phase images showed that the surface of shaved MV and reconstituted MV were different than native MV, as indicated by the presence of protrusions (darker areas found on the vesicles' surface) with distinct viscoelastic features (Table 1, Figure 3). The presence of protrusions on the surface of shaved MV and reconstituted MV, but not on native MV, could indicate protein aggregation or changes in lipid composition.

Next, we investigated the ability of MV groups to mineralize in vitro by turbidimetry assay (Table 2, Figure 4A-B). Mineral propagation induced by vesicles was studied under 2 incubation conditions: with P_i and with ATP. A sigmoidal behavior was observed for mineralization curves under both conditions for all groups.

In the evaluation of nucleation potential under favorable concentration of Ca^{2+} and P_i , shaved MV exhibited a delay in the mineral initiation and propagation, with a 40% reduction in the potential of mineral propagation compared to MV counterparts. Reconstituted MV behavior was similar to native MV regarding the initial and final time of mineralization, however, the potential of mineral propagation ($\text{U}_{\text{max}}/\text{t}_{\text{max rate}}$) was the lowest one between groups (Table 2, Figure 4A).

When using ATP as substrate, which reflects the physiological MV capacity to hydrolyze ATP and generate P_i , shaved MV had the lowest potential of mineral propagation, although it was the reconstituted MV that exhibited a delay in 30% in initial time of mineralization compared to native MV (Table 2, Figure 4B).

Furthermore, the mineral formed by each group of MV was characterized using ATR-FTIR spectroscopy (Figure 4C). Similar ATR-FTIR spectra patterns, assigned to the precipitation of calcium phosphates irrespective of the sample, were

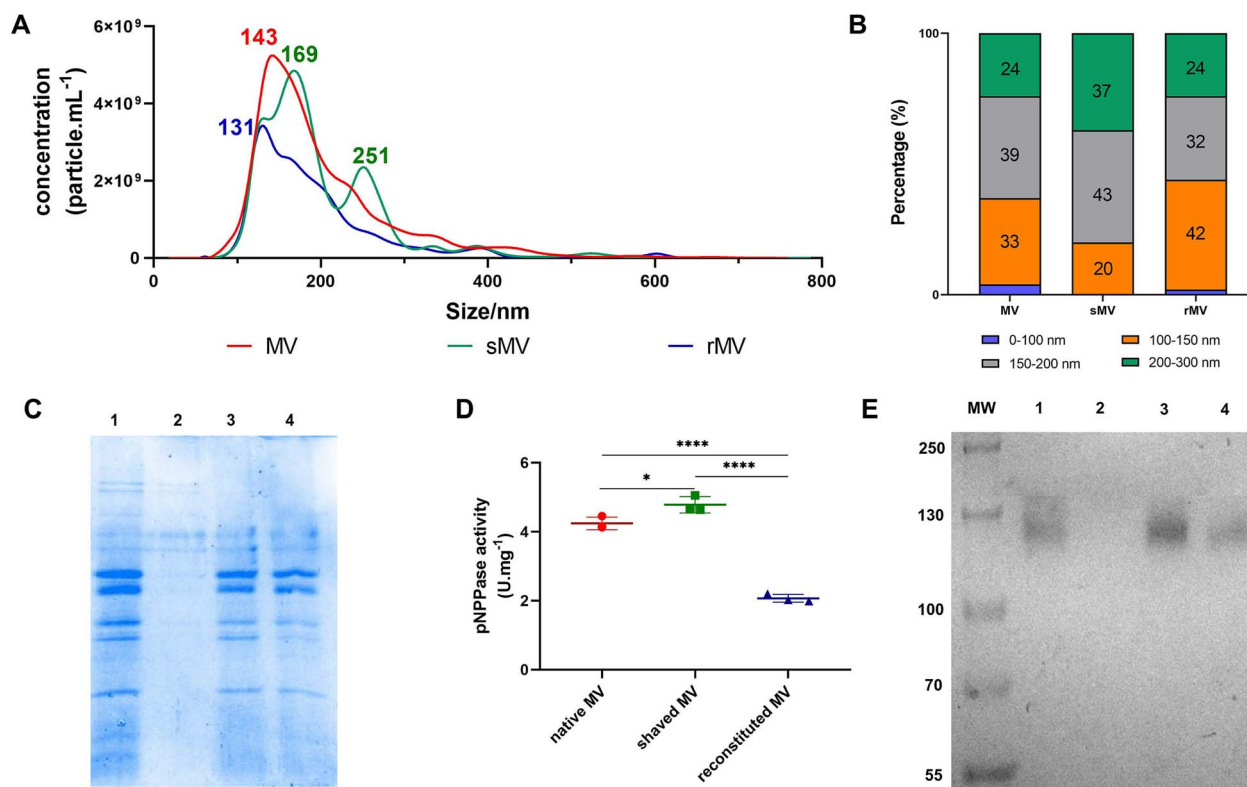


Figure 2. Biophysical and biochemical characterizations of native MV, shaved MV, and reconstituted MV. (A, B) Size distribution measured by nanoparticle tracking analysis (NTA NS3000, Malvern). (C) Protein profiles by SDS-PAGE on 12% polyacrylamide gel. (D) TNAP specific activity. (E) TNAP specific activity on 7% polyacrylamide renatured gel. Lane numbers at the top of gels corresponds to: (1) native MV; (2) protein corona removed by high ionic strength; (3) shaved MV; and (4) reconstituted MV. Abbreviations: MV, matrix vesicle; MW, molecular weight standards; TNAP, tissue nonspecific alkaline phosphatase.

Table 2. MV kinetic parameters obtained from the mineralization curves, incubated with P_i and ATP as nucleators for 20 hr.

Mineralization parameters		t_i (hr)	t_f (hr)	$t_{max\ rate}$ (hr)	U_{max}	$U_{max}/t_{max\ rate}$ (hr ⁻¹)
ATP	Native MV	4.61 ± 0.2	20 ± 0.3	10.78 ± 2	0.298 ± 0.005	0.028 ± 0.003
	Shaved MV	5.17 ± 0.03	16.3 ± 0.2	10 ± 2	0.143 ± 0.007	0.014 ± 0.003
	Reconstituted MV	6 ± 0.25	20 ± 0.3	12.4 ± 2	0.285 ± 0.006	0.024 ± 0.003
P _i	Native MV	0.85 ± 0.02	3.43 ± 0.07	1.31 ± 0.03	0.296 ± 0.003	0.225 ± 0.003
	Shaved MV	1.77 ± 0.04	4.68 ± 0.09	2.04 ± 0.04	0.269 ± 0.005	0.131 ± 0.003
	Reconstituted MV	0.87 ± 0.02	3.58 ± 0.07	1.25 ± 0.02	0.236 ± 0.004	0.188 ± 0.002
Statistical analysis (<i>p</i> value)						
ATP	MV × sMV	0.0241	<0.0001	0.0279	<0.0001	0.0033
	MV × rMV	0.0003	0.4184	0.0001	0.0866	0.4280
	sMV × rMV	0.0047	<0.0001	<0.0001	<0.0001	0.0124
P _i	MV × sMV	<0.0001	<0.0001	<0.0001	0.0005	<0.0001
	MV × rMV	0.6368	0.1368	0.1215	<0.0001	<0.0001
	sMV × rMV	<0.0001	<0.0001	<0.0001	0.0002	<0.0001

Abbreviations: MV, matrix vesicles; t_i , initial time of mineral formation; t_f , final time of mineral formation; $t_{max\ rate}$, time at maximum rate of mineral formation; U_{max} , maximum value of turbidity; (U_{med}); $U_{max}/t_{max\ rate}$, potential of mineral propagation. Data are reported as mean ± SD. Two-way ANOVA followed by Tukey's test was applied and *p* value < 0.05 was considered statistically significant (bold).

observed. The bands from 1800 to 1200 cm⁻¹ are assigned to carbonyl and amide groups from the organic compounds.³⁷ The 2 intense bands in the range of 1100 to 960 cm⁻¹ are assigned to the formation of poor crystalline calcium phosphates and/or phosphate in acidic environment.³⁸ The band centered at 1040-1030 cm⁻¹ is assigned to the asymmetric stretching of the PO₄³⁻ group, which may correspond to apatite.³⁷ The band centered at 985 cm⁻¹ is assigned to the HPO₄²⁻ group, which may indicate the presence of brushite. The low-intensity band at 925 cm⁻¹ is assigned to the P-O-P group.³⁸ The set of bands at lower wavenumber is used as

fingerprints of HAp structure. The doublet at 600-560 cm⁻¹ is characteristic of crystalline phosphate phases.³⁷ It is important to note the better definition of the peaks in the doublet in the MV samples, which indicates the formation of more crystalline phase compared to shaved MV and reconstituted MV.

To determine whether shaving the protein corona alters the anchoring of MV to a collagen-rich organic ECM, we evaluated the specific interaction ability of native MV, shaved MV, and reconstituted MV with collagen-based scaffolds (Figure 5). SEM analysis of native MV after 48 hr of incubation on collagen-based scaffolds, in the absence of ATP,

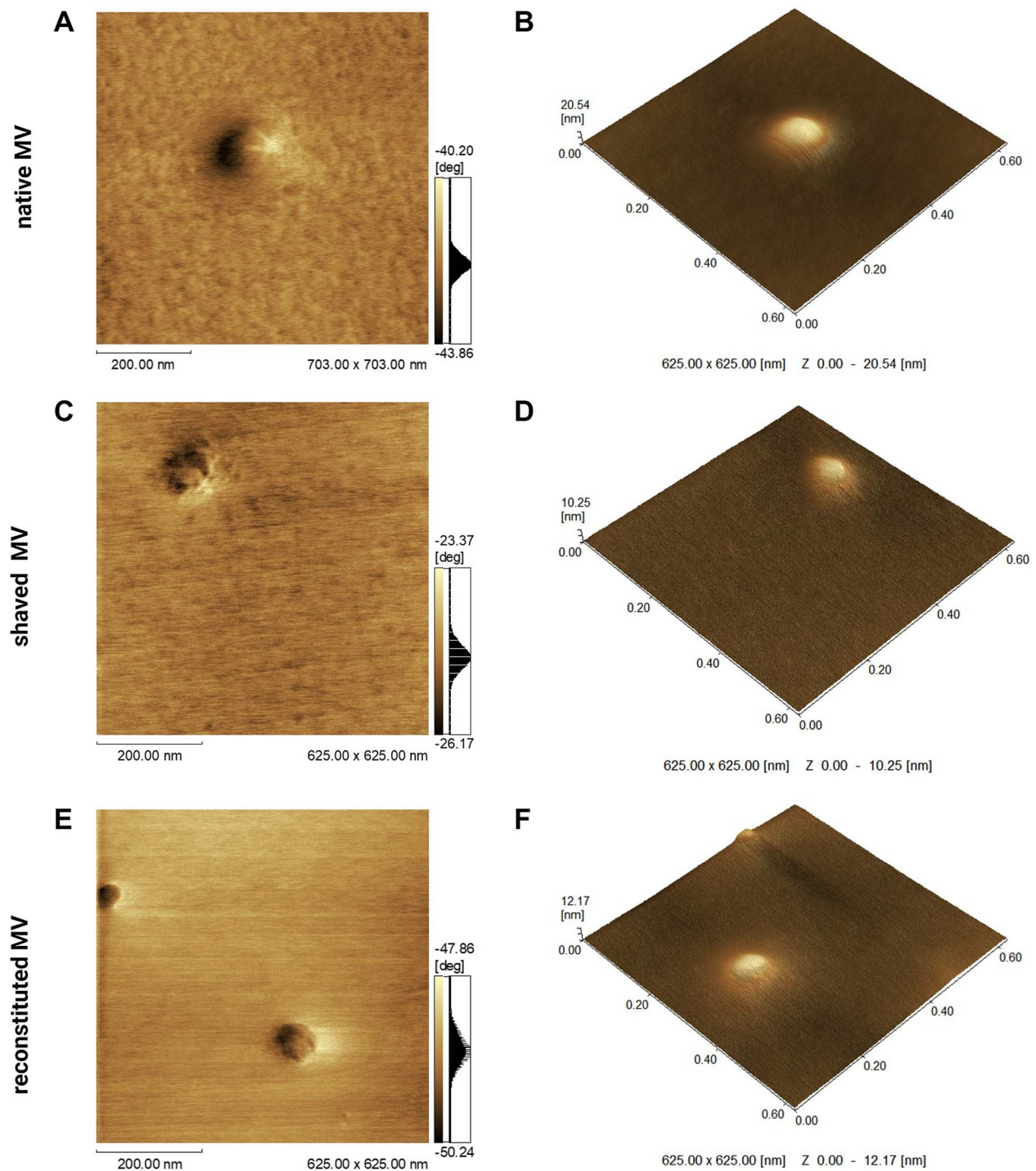


Figure 3. AFM micrographs of MV groups. (A, B) Native MV. (C, D) Shaved MV. (E, F) Reconstituted MV. (A, C, and E) Phase image showed short range of phase shift in the vesicle's topology, revealing a high protein complexity. (B, D, and F) 3D topographic image showed the vesicle's topology. Images were obtained using a Shimadzu SPM-9600 scanning probe microscopy (Shimadzu, Japan). For each sample, 100 vesicles were analyzed. Abbreviations: AFM, atomic force microscopy; MV, matrix vesicle.

showed spheroidal structures with diameters ranging from 104 to 177 nm, anchored to the organic matrix (Figure 5A). However, in the presence of ATP, a morphological change was evident (Figure 5B), which could be associated with the propagation of mineral promoted by the native MV embedded in the collagen-based scaffold. Additionally, the number of vesicles embedded in the collagen-based scaffold was higher

(Figure 5B), indicating that the mineralization process was accelerated.

In contrast, shaved MV did not anchor to the collagen-based scaffolds, regardless of the presence or absence of ATP (Figure 5C, D). Only collagen fibrils were observed, without any indication of the morphological changes observed in native MV, indicating that without the anchoring of shaved

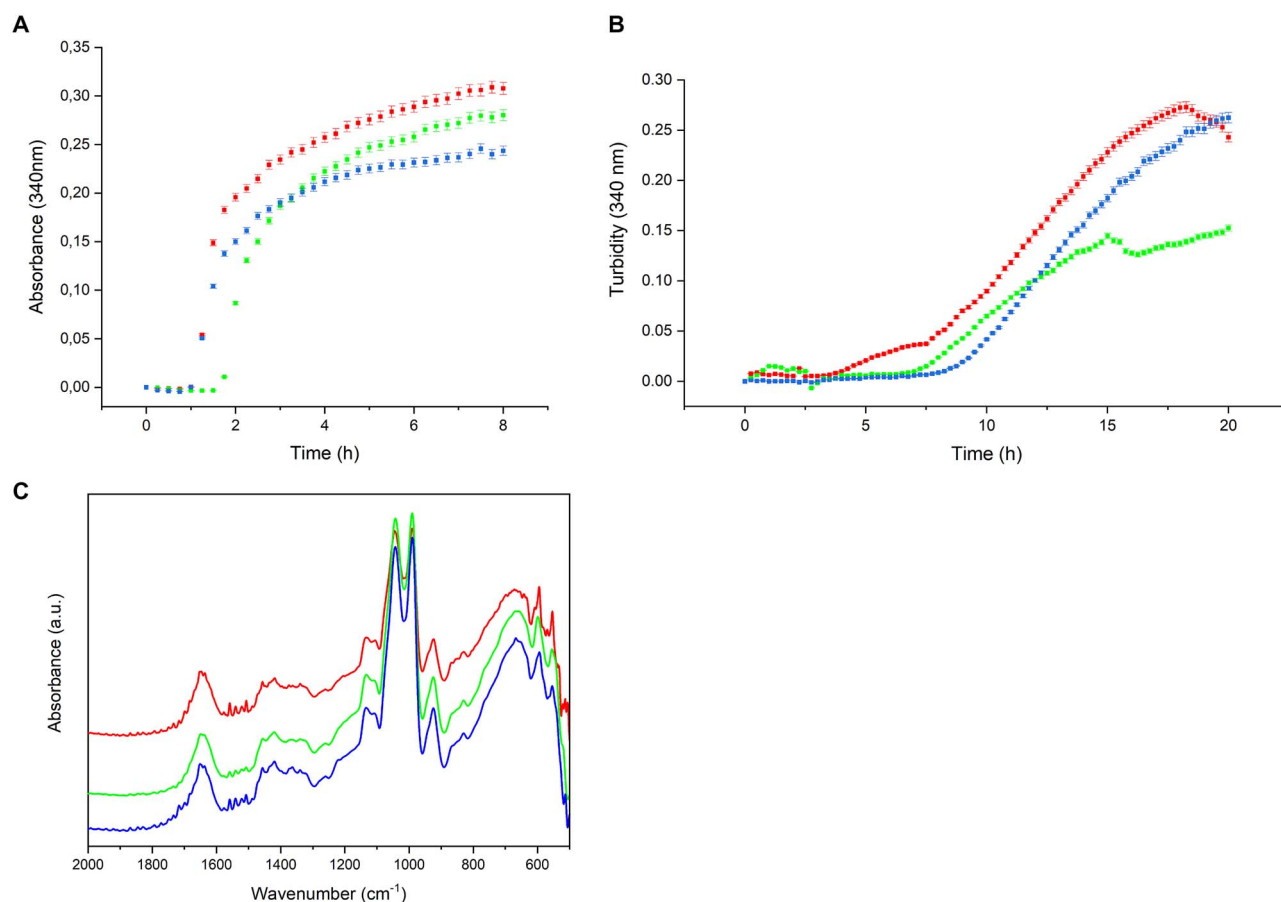


Figure 4. In vitro mineralization and mineral characterization of MV groups. Native MV (red); shaved MV (green) and reconstituted MV (blue). Mineralization curves in the presence of Pi (A) and ATP (B). (C) ATR-FTIR spectra of minerals produced by vesicles in the presence of ATP. Data reported as the mean of triplicate measurements. Abbreviation: MV, matrix vesicle.

MV, the deposition and propagation of the mineral phase did not occur.

Interestingly, the incubation of reconstituted MV with the collagen-based scaffold restored their anchoring ability (Figure 5E, F), comparable to that of native MV. This suggested that the inherited ability of MV to anchor to the scaffold seems to return once the protein corona was partially reconstituted, along with the capacity to mineralize this collagenous ECM. Thus, in the presence of ATP (Figure 5F), reconstituted MV promoted a remarkable advanced stage of mineral deposition into the collagen-based scaffold, specifically HAp as attested by FTIR analysis (Figure 4C). However, the formed mineral was in an earlier stage compared to the mineralization achieved by native MV.

Proteomic analysis of vesicles

The 3 groups of MV underwent proteomics analysis, resulting in the identification of 2,848 gene products (full list provided in Table S1). Principal component analysis (PCA) was performed to compare possible variances between the groups (Figure 6A). The results showed that the vesicles formed distinct groups, with shaved MV and reconstituted MV being more similar to each other compared to native MV.

Regarding the expression of proteins known to contribute to the mineralization process, no differences in their intensities were observed among groups. These proteins include phosphatases: TNAP (or ALPL), members of the

Ectonucleotide Pyrophosphatase/Phosphodiesterase family (ENPP-1, -3, -4, and -6) and Phosphoethanolamine/Phosphocholine Phosphatase 1 (PHOSPHO1); members of the Annexins family (A1, A2, A4-7, and A8L1); sphingomyelin phosphodiesterases (SMPD1 and SMPD3); phosphate transporters (SLC20A1/PiT1 and SLC20A2/PiT2); vitronectin (VTN); carbonic anhydrases (CA12 and CA2); and members of the integrin beta Family (ITGB1-5). Interestingly, the process of protein corona shaving resulted in the removal of certain types of collagens (COL9A3, COL5A1, and COL12A1). No statistical difference was observed in the relative expression between shaved MV and reconstituted MV, indicating that the reconstitution of these collagens was not possible. However, we observed that the relative presence of these collagens was slightly less decreased in reconstituted MV compared to shaved MV. This result corroborated our collagen anchoring assay, in which we did not observe any interactions between shaved MV with the collagen-based scaffold, whereas reconstituted MV partially recovered that ability.

Differential protein composition among MV groups was analyzed, and each protein was classified as a hit, a candidate, or a no hit (Figure 6B, Tables S2 and S3).

In the comparative proteomic analysis of shaved MV and native MV, a total of 161 hit proteins were identified. Among these, 135 proteins were decreased, while 26 proteins exhibited higher abundance in shaved MV (Figure 6C). Similarly, when comparing reconstituted MV with native MV, a total

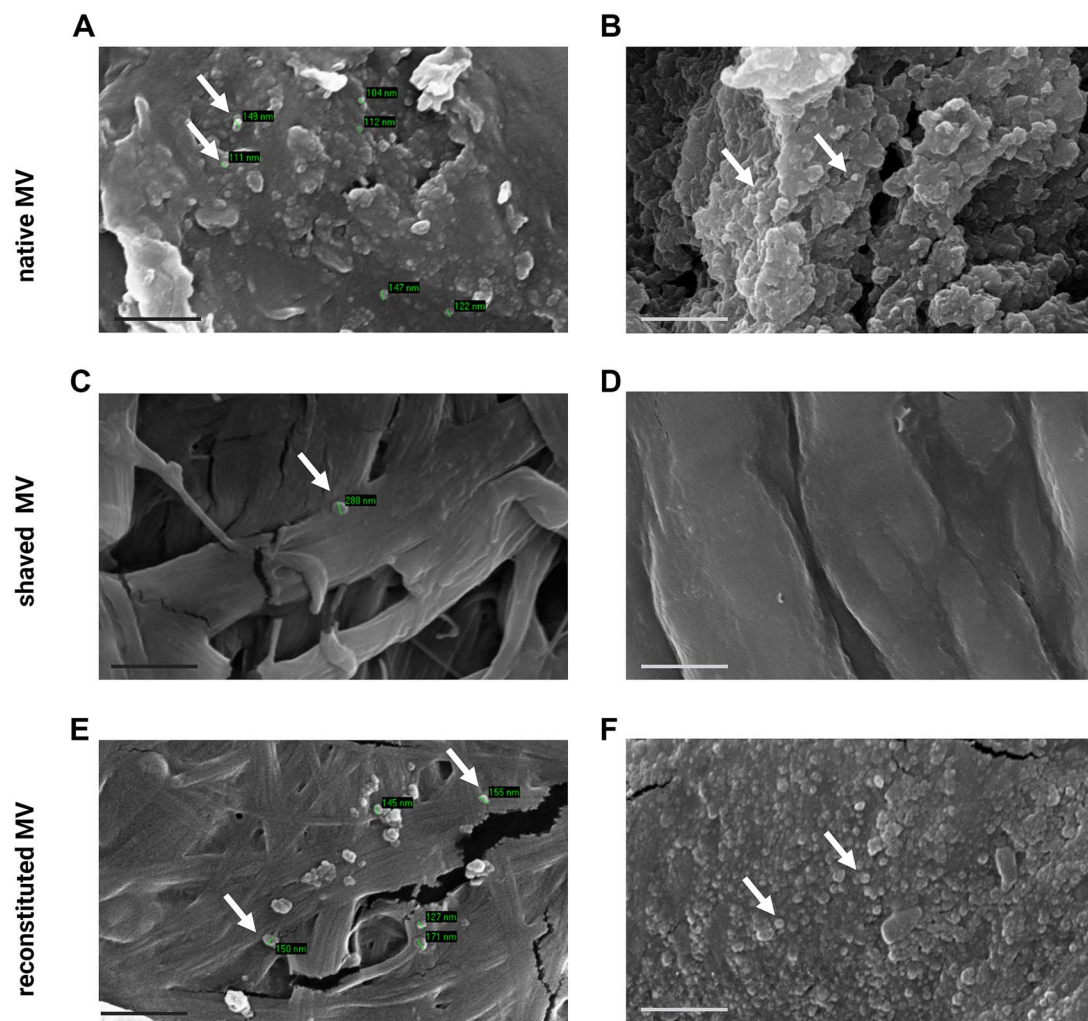


Figure 5. Electron microscopy images of the collagen-based scaffolds incubated with MV groups. The assay was performed in the absence (A, C, and E) and presence (B, D, and F) of ATP. Micrographs obtained at 15 000 \times magnification (A, C, and E), the black scale bar represents 1 μ m, whereas in the images captured at 8000 \times magnification (B, D, and F), the white scale bar represents 2 μ m. White arrows indicate the interaction of the vesicles with the organic matrix. Abbreviation: MV, matrix vesicle.

of 112 hit proteins were identified, with 79 proteins showing decreased abundance and 33 proteins displaying increased abundance in reconstituted MV (Figure 6C). The comparison of the ratios of shaved native MV with reconstituted native MV, referred to here as the comparison between shaved MV and reconstituted MV, revealed 36 hit proteins, with 32 downregulated and 4 upregulated in shaved MV (Figure 6C).

Notably, the Histone H2A.V (H2AZ2) protein was consistently identified as a hit protein in all comparisons and was the most decreased in shaved MV compared to native MV, followed by SET and Isovaleryl-CoA dehydrogenase (IVD). The proteins SET, LOXL3, and LYZ showed some of the lowest abundance in both shaved MV and reconstituted MV compared to native MV.

A total of 553 proteins were considered hit or candidate in at least one of the comparisons (full list provided in Table S3), and the heatmap of these proteins, separated by each vesicle group, shows the pattern of proteins removed by the high ionic strength treatment in shaved MV, as well as the pattern of proteins in reconstituted MV samples (Figure 6D).

Next, we conducted gene ontology analysis (GO) (Figure S1) to identify the biological processes, cellular compartments, and molecular functions of these 553 proteins, focusing on those that were decreased in the comparisons between: (1) shaved MV and native MV; (2) reconstituted MV and native MV; (3) shaved MV and reconstituted MV.

The GO for biological process revealed that in the comparison with native MV, both in shaved MV and in reconstituted MV, the decreased proteins were associated with external encapsulating structure organization, negative regulation of proteolysis, organization of ECM and extracellular structure, and carboxylic/organic acid catabolic processes. Following the significance comparison with native MV, we observed a decrease of proteins associated with the regulation of endopeptidase and peptidase activity only in shaved MV, while in reconstituted MV, the decreased proteins were related to small molecule and cellular amino acid catabolic processes, cytoplasmatic translation and collagen fibril organization. In addition, the comparison of shaved MV and reconstituted MV indicates a partial reconstitution of proteins related to epithelial cell-cell adhesion,

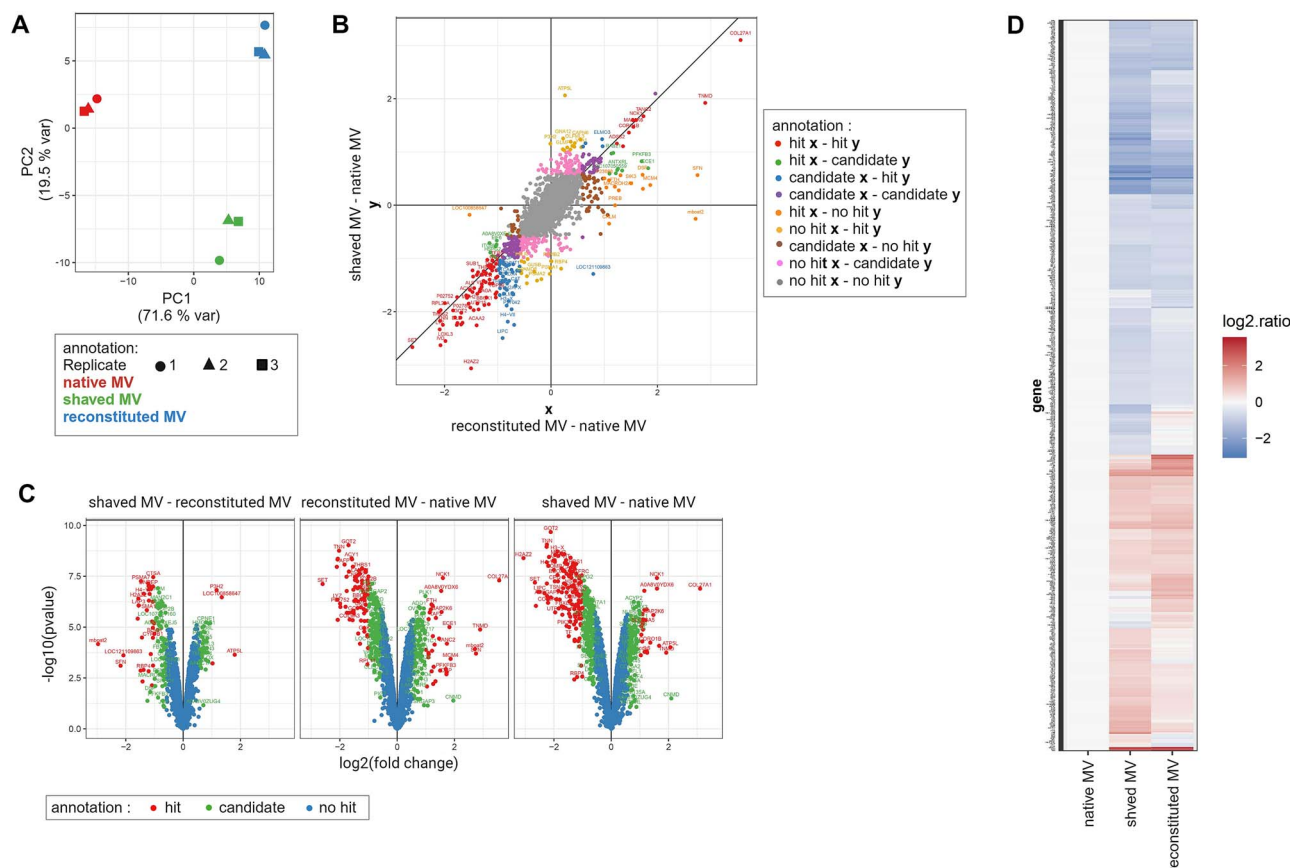


Figure 6. Comparative proteomic analysis of MV groups. The analyzed comparisons were shaved MV with native MV, reconstituted MV with native MV, and the ratio of (shaved MV with native MV) to (reconstituted MV with native MV). (A) PCA analysis showing the possible variance and group differences. (B) Fold change correlation of all differential proteins classified in hit, candidate, and no hit proteins. A hit protein was defined as one with an FDR below 5% and a resulting fold-change of at least 100%. A candidate protein was defined as having an FDR below 20% and a resulting fold change of at least 50%. Proteins that did not meet these criteria were considered “no hit.” Proteins were tested for differential expression using a moderated t-test by applying the limma package.³⁵ (C) Volcano plot of hit, candidate, and no hit protein. (D) Heatmap analysis of 553 downregulated proteins founded in shaved MV and reconstituted MV. Abbreviations: FDR, false discovery rate; MV, matrix vesicle; PCA, principal component analysis.

proteasome-mediated ubiquitin-dependent protein catabolic processes, and monosaccharide/hexose metabolic processes.

Regarding the GO for cellular compartment, focusing on comparisons with native MV that were significant in both shaved MV and reconstituted MV, we found a decrease of proteins associated as components of secretory granule lumen, cytoplasmic vesicle lumen, vesicle lumen, and collagen-containing ECM. Likewise, shaved MV showed downregulation in proteins that compose proteasome core complex, vacuolar lumen, primary lysosome, and azurophil granule. In reconstituted MV comparison with native MV, proteins described as part of the basement membrane, cytosolic ribosome, and ribosomal subunits were decreased. Interestingly, by analyzing the decreased proteins resulting from the shaved MV comparison with reconstituted MV, we determined a partial reconstitution of proteins from the secretory granule lumen, cytoplasmic vesicle lumen, vesicle lumen, proteasome core complex, endopeptidase and peptidase complex, and ficolin-1 rich granule complex.

In the comparisons with native MV, the GO for molecular function showed that most of the decreased proteins in shaved MV were related to the activity of peptidase, exopeptidase, endopeptidase, and aminopeptidase. In reconstituted MV, decreased proteins were mainly associated with sulfur compound binding, collagen anchoring, ribosomal constituents,

integrin binding, and rRNA binding, compared to native MV. Proteins associated to ECM structural constituents, enzyme inhibitory activity, glycosaminoglycan binding, and heparin binding, were decreased in shaved MV and reconstituted MV compared to native MV. Finally, proteins associated with heterotypic cell-cell adhesion, ECM structural components, hydrolase activity, and the activity of exopeptidase, peptidase, endopeptidase aminopeptidase, and carboxypeptidase, were decreased in shaved MV compared to reconstituted MV.

Discussion

In the field of synthetic nanoparticles, the spontaneous adsorption of molecules present in biofluids onto the nanoparticles surface is a well-known concept considered essential to guarantee the expected response or effect. The same ability to incorporate a protein corona on their surface was also reported for natural nanoparticles as EV.^{15,18,20,39}

In this context, we found that the different protein compositions related to the presence or absence of a protein corona alter the MV biochemical and biophysical properties. Moreover, the protein corona mediates the interaction between MV with the ECM and modulates their enzymatic machinery. It is important to highlight that we defined the protein corona as the set of proteins removed after incubation in a high

ionic strength solution, which may include proteins both pre-assembled by parent cells (cell-derived) and acquired from tissue fluid.

Wolf and collaborators¹⁶ studied the protein corona present in EV derived from human placental-expanded stromal cells. The protein corona was enriched with proangiogenic factors, and their removal by size-exclusion or ultracentrifugation resulted in a loss of proangiogenic potential. The authors reconstituted the protein corona by incubating the shaved EV with the proangiogenic factors, which resulted in the re-establishment of the angiogenic ability. However, this effect was minor compared to the native protein corona activity.¹⁶

In a similar approach, the formation of protein corona in mesenchymal stem cells EV was investigated in an in vitro model. Hard protein corona was drastically removed by using 2% w/v SDS, 62.5 mM Tris-HCl solution, followed by incubation at 95°C. The culture conditions influenced hard protein corona composition, and the authors observed that exogenous proteins present in fetal bovine serum (or its equivalent), mainly bovine albumin, were adsorbed on EV surface, and even under serum free conditions, the presence of protein corona was reported. Despite that, the presence of bovine albumin in protein corona led to an increase in EV uptake by target cells and a reduction in EV clearance by phagocytic cells.³⁹ Although using a different strategy to remove the protein corona, these 2 studies point to the important influence of a protein corona on EV function.

High levels of TNAP activity are a defining property of mineralization-competent MV.^{12,40} We observed that the removal of the protein corona led to an increase in TNAP specific activity, and that reconstitution of the protein corona was not able to restore the activity to native MV levels. However, in the mineralization assays under condition that mimics a physiological osteogenic microenvironment (using ATP as a source to P_i), we observed that the enzymatic machinery was affected in shaved MV, including TNAP activity, with a remarkable reduction in the mineralization potential. TNAP activity alone did not lead to greater mineral formation, and the activity variation may reflect changes in the enzyme conformation promoted or modulated by the adherence of surface proteins.

Interestingly, the minerals produced by shaved MV and reconstituted MV did not show the formation of more crystalline phase as observed in native MV. Taking this result along with the mineralization assay, we observed a modulation in MV role during the initial formation and mineral nucleation after the removal of protein corona. Although partially recovered in reconstituted MV, the removal of protein corona affected the quality of the produced mineral.

Mineral propagation on ECM depends on the interaction between MV with the collagenous ECM. This anchoring ability has been linked to Annexins (A5 and A6),^{8,41} TNAP,⁴¹ and integrins, a family of transmembrane proteins which may mediate several key processes, as both cell- and/or vesicle-ECM interactions.^{2,42} We found that the protein corona was associated with the MV mineralizing capabilities, not only aiding in the anchoring but also playing a role in mineral nucleation and propagation. In addition, the protein corona seems to also modulate TNAP collagen-binding capacity.

We acknowledge the interspecies nature of our system, using MV from chick embryos and collagen scaffolds derived from murine tails, as a potential limitation. While Type I collagen is highly conserved across species, subtle differences in

ECM-associated proteins or post-translational modifications could influence vesicle-matrix interactions. Despite this, our results indicate that the removal or absence of the protein corona is the primary factor affecting MV anchoring ability, independent of interspecies compatibility. This highlights the robustness of the protein corona in mediating vesicle-matrix interactions and provides insights into its critical molecular role. Future studies employing species-matched models will further validate and extend these findings, exploring the potential impact of interspecies differences.

Our results suggest that the anchoring ability is partially related to type V (COL5A1 subunit), IX (COL9A3 subunit), and XII (COL12A1 subunit) collagens. COL5A1 and COL12A1 interact with type I collagen, the most abundant organic component in the bone ECM^{43,44} while COL9A3 is known to interact with type II and IX collagens.⁴⁵ The binding to proteoglycans, such as biglycan, decorin, and aggrecan, was associated with COL5A1 and COL9A3, respectively. These interactions are important for the regulation of fibrillogenesis and ECM organization. In addition, both COL12A1 and COL9A3 bind to integrins $\alpha 1\beta 1$ and $\alpha 2\beta 2$, a process associated with adhesion to the ECM.⁴⁶ Mutations in COL5A1, COL9A3, and COL12A1 were described in connective tissue disorders, such as Ehlers–Danlos syndromes, multiple epiphyseal dysplasia, osteoarthritis, and intervertebral disk disease.⁴⁷ Further studies are necessary to determine whether the loss of anchoring ability to type I collagen ECM is mediated by one or more of these 3 subunits.

A limitation of this study is that the reestablishment of the anchoring ability and mineralization potential in reconstituted MV was not completely equivalent to that of native MV. This partial reconstitution could be due to several factors: irreversible aggregation of certain protein components after removal from the MV, loss of certain protein components due to dialysis, altered order of binding and changes in the stoichiometric proportions of the shaved proteins when added back to the rMV.

Although the precise mechanisms of MV interaction with ECM biomolecules and how these vesicles participate in the architecture and remodeling of the mineralized ECM cannot yet be fully elucidated in this study, the effect of protein corona removal on the ability of MV to mineralize and bind to collagen fibers was demonstrated. The proteomic results showed the removal of proteins related to external structural and ECM organization, regulation of peptidase activity and with carboxylic/organic acid catabolic processes. Indeed, the top 3 downregulated proteins in shaved MV were H2AZ2 (Histone H2A.V), SET, and IVD (Isovaleryl-CoA dehydrogenase). H2AZ2 and SET participate in cell adhesion, vesicle-mediated processes, and membrane organization, while IVD is involved with catabolic processes.⁴⁸ Interestingly, most of the EV-associated proteins observed in our samples were related to ectosomes, which support the hypothesis that MV are generated from the budding of plasma membranes as described.^{1,5}

Using human osteosarcoma Saos-2 cells, Thouverey and colleagues compared proteome differences between released MV and their apical microvilli cell counterpart. The authors observed that a group of unique proteins only present in MV, related to ECM, signal transduction, enzyme activity, membrane traffic, and protein regulation.⁴⁹ These findings suggested the presence of adsorbed proteins onto the MV's surface, as discussed in a recent review.¹³ We searched for

these proteins (including different family members) in our MV, and most of the proteins were not differently present in native MV, shaved MV, and reconstituted MV, such as chondroitin sulfate proteoglycan 2, cysteine-rich angiogenic inducer 61, syndecan 2, syntaxin 4A, and vitronectin. This could be due to the different cellular type, species, and context (protein corona derived from medium supernatant) but could also be related to the different region of the plasma membrane from which MV originated. However, lactate dehydrogenases (LDH; LDHA and LDHB) and alpha-2 macroglobulin (A2M) were down-regulated in shaved MV and reconstituted MV, corroborating that these proteins were part of the set of adsorbed protein corona. LDH primary function is glycolysis and energy metabolism. Interestingly, those proteins were associated with extracellular processes, including the regulation of collagen deposition.⁵⁰ This regulation may be explained by: (1) providing a secondary energy source (anaerobic) which sustains the ATP-energy necessary to collagen production; (2) reducing the pH of ECM due lactate production, which downregulates collagen secretion into ECM; (3) regulating the activity of metalloproteinases. Similarly, A2M protein is associated with metalloproteinases inhibition, resulting in accumulation of collagen type I and IV.⁵⁰

Heidarzadeh and colleagues reviewed the protein corona interference in exosomes activity, highlighting that the nature and type of proteins and metabolites incorporated into the protein corona layer depend on the biofluid to which vesicles are exposed.²⁰ In addition, minimal changes in pH and temperature have the potential to change the 3D folding of incorporated protein corona, which in turn affects their activity.²⁰ It is crucial to standardize not only the applied method for EV isolation, but also the characteristics of the buffer, medium, and other solutions (such as pH, temperature, and ionic strength) used, as they can directly affect the protein corona.

In conclusion, this work demonstrates for the first time that the protein corona is important for the proper functioning of MV during biomineralization and that the presence of TNAP activity alone is insufficient for effective mineralization and mineral propagation into ECM, as the presence and composition of a protein corona influences TNAP's enzymatic activity. Furthermore, the formation of a protein corona proved crucial for collagen binding. Further investigations are required to elucidate each corona protein origin (whether cell-derived or acquired from biological fluids), and the regulation of protein corona adsorption and activity, including the anchoring to ECM and mineralization processes. Altogether, our findings provide novel valuable insights that pave the way for the future development of advances in biomimetic materials and bone regeneration medicine applications using protein corona.

Acknowledgments

Thank you to Per Haberkant and Frank Stein, from the Proteomics Core Facility, of the European Molecular Biology Laboratory, in Heidelberg, Germany; and to Ivana Borin from the AFM Core Facility, of the FFCLRP-USP multiuser platform.

Author contributions

Juçara Gastaldi Cominal, Heitor Gobbi Sebinelli (Formal analysis, Investigation, Methodology, Writing—review & editing), Larwsk

Hayann, Lucas Fabrício Bahia Nogueira (Formal analysis, Data curation, Writing—review), Marcos Antonio Eufrásio Cruz (Formal analysis, Methodology, review), Maryanne Trafanni Mello, Luiz Henrique da Silva Andrilli, Maytê Bolean (Formal analysis, Methodology, Data curation, review), Saida Mebarek, Massimo Bottini, Ana Paula Ramos, José Luis Millán, Pietro Ciancaglini (Conceptualization, Resources, Supervision, Writing—review & editing). All authors approved the final manuscript. Juçara Gastaldi Cominal and Heitor Gobbi Sebinelli contributed equally to this work. Juçara Gastaldi Cominal (Formal analysis, Investigation, Methodology, Writing—review & editing), Heitor Gobbi Sebinelli (Formal analysis, Investigation, Methodology, Writing—review & editing), Larwsk Hayann (Data curation, Formal analysis, Writing—review & editing), Lucas Fabrício Bahia Nogueira (Data curation, Formal analysis, Writing—review & editing), Marcos Antonio Eufrásio Cruz (Formal analysis, Methodology, Writing—review & editing), Maryanne Trafanni Mello (Data curation, Formal analysis, Methodology, Writing—review & editing), Luiz Henrique da Silva Andrilli (Data curation, Formal analysis, Methodology, Writing—review & editing), Maytê Bolean (Data curation, Formal analysis, Methodology, Writing—review & editing), Ana Paula Ramos (Conceptualization, Resources, Supervision, Writing—review & editing), Saida Mebarek (Conceptualization, Resources, Supervision, Writing—review & editing), Massimo Bottini (Conceptualization, Resources, Supervision, Writing—review & editing), Jose Luis Millan (Conceptualization, Resources, Supervision, Writing—review & editing), and Pietro Ciancaglini (Conceptualization, Resources, Supervision, Writing—review & editing)

Supplementary material

Supplementary material is available at *JBMR Plus* online.

Funding

The authors acknowledge the funding from: Fundação de Amparo à Pesquisa do Estado de São Paulo (FAPESP), grants 2019/08568-2 (to P.C.); 2019/25054-2 (to A.P.R.); 2021/13140-1 (to L.H.S.A.); 2022/04885-6 (to J.G.C.); 2022/05026-7 (to H.G.S.); 2023/17960-9 (to L.H.); Coordenação de Aperfeiçoamento de Pessoal de Nível Superior (CAPES) grants Finance Code 001 (to A.P.R. and P.C.); 88887.320304/2019-00 (to M.B.); Conselho Nacional de Desenvolvimento Científico e Tecnológico (CNPq) grants 305426/2021-4 (to P.C.); PVE-Print CAPES-USP 2020-88887.569449/2020-00 (to A.P.R.) and Brazil-France USP-COFECUB Uc Sv 184/20 grant; Italian Ministry for Research (to P.C. and S.M.) [2022 Program for Research Projects of National Interest (PRIN), Grant # 20229RMZZW] (to Mas. B.) and grant P01 AG081167 from the National Institute of Ageing, National Institutes of Health, USA (to J.L.M.). P.C. and A.P.R. are CNPq researchers.

Conflicts of interest

None declared.

Data availability

Processed data will be made available upon reasonable request.

References

1. Wuthier RE, Lipscomb GF. Matrix vesicles: structure, composition, formation and function in calcification. *Front Biosci.* 2011;16(1):2812–2902. <https://doi.org/10.2741/3887>
2. Anderson HC. Matrix vesicles and calcification. *Curr Rheumatol Rep.* 2003;5(3):222–226. <https://doi.org/10.1007/s11926-003-0071-z>

3. Plaut JS, Strzelecka-Kiliszek A, Bozycki L, et al. Quantitative atomic force microscopy provides new insight into matrix vesicle mineralization. *Arch Biochem Biophys*. 2019;667:14–21. <https://doi.org/10.1016/j.abb.2019.04.003>
4. Buchet R, Pikula S, Magne D, Mebarek S. Isolation and characteristics of matrix vesicles. In: Millán JL, ed. *Phosphatase Modulators*; Methods in Molecular Biology. Vol. 1053. Totowa: Humana Press; 2013:115–124 ISBN 978-1-62703-561-3 10.1007/978-1-62703-562-0_7.
5. Mebarek S, Buchet R, Pikula S, et al. Do media extracellular vesicles and extracellular vesicles bound to the extracellular matrix represent distinct types of vesicles? *Biomolecules*. 2024;14(1):42. <https://doi.org/10.3390/biom14010042>
6. Hsu HHT, Anderson CH. A role for ATPase in the mechanisms of ATP-dependent Ca and phosphate deposition by isolated rachitic matrix vesicles. *Int J Biochem Cell Biol*. 1995;27(12):1349–1356. [https://doi.org/10.1016/1357-2725\(95\)00103-V](https://doi.org/10.1016/1357-2725(95)00103-V)
7. Wuthier RE, Chin JE, Hale JE, Register TC, Hale LV, Ishikawa Y. Isolation and characterization of calcium-accumulating matrix vesicles from chondrocytes of chicken epiphyseal growth plate cartilage in primary culture. *J Biol Chem*. 1985;260(29):15972–15979. [https://doi.org/10.1016/S0021-9258\(17\)36354-8](https://doi.org/10.1016/S0021-9258(17)36354-8)
8. Veschi EA, Bolean M, da Silva Andrilli LH, et al. Mineralization profile of Annexin A6-harboring proteoliposomes: shedding light on the role of Annexin A6 on matrix vesicle-mediated mineralization. *Int J Mol Sci*. 2022;23(16):1–15. <https://doi.org/10.3390/ijms23168945>
9. Millán JL. The role of phosphatases in the initiation of skeletal mineralization. *Calcif Tissue Int*. 2013;93(4):299–306. <https://doi.org/10.1007/s00223-012-9672-8>
10. Sebinelli HG, Henrique L, Andrilli S, et al. Shedding light on the role of Na, K-ATPase as a phosphatase during matrix-vesicle-mediated mineralization. *Int J Mol Sci*. 2022;23(23):15072. <https://doi.org/10.3390/ijms232315072>
11. Bolean M, Izzi B, van Kerckhoven S, et al. Matrix vesicle biomimetics harboring Annexin A5 and alkaline phosphatase bind to the native collagen matrix produced by mineralizing vascular smooth muscle cells. *Biochim Biophys Acta Gen Subj*. 2020;1864(8):1–9. <https://doi.org/10.1016/j.bbagen.2020.129629>
12. Shapiro IM, Landis WJ, Risbud MV. Matrix vesicles: are they anchored exosomes? *Bone*. 2015;79:29–36. <https://doi.org/10.1016/j.bone.2015.05.013>
13. Ramos AP, Sebinelli HG, Ciancaglini P, et al. The functional role of soluble proteins acquired by extracellular vesicles. *J Extracell Biol*. 2022;1(1):e34. <https://doi.org/10.1002/jex2.34>
14. Mahmoudi M, Landry MP, Moore A, Coreas R. The protein corona from nanomedicine to environmental science. *Nat Rev Mater*. 2023;8(7):422–438. <https://doi.org/10.1038/s41578-023-00552-2>
15. Dietz L, Oberländer J, Mateos-Maroto A, et al. Uptake of extracellular vesicles into immune cells is enhanced by the protein corona. *J Extracell Vesicles*. 2023;12(12):e12399. <https://doi.org/10.1002/jev2.12399>
16. Wolf M, Poupardin RW, Ebner-Peking P, et al. A functional corona around extracellular vesicles enhances angiogenesis, skin regeneration and immunomodulation. *J Extracell Vesicles*. 2022;11(4):1–20. <https://doi.org/10.1002/jev2.12207>
17. Singh P, Szigyártó IC, Ricci M, et al. Removal and identification of external protein corona members from RBC-derived extracellular vesicles by surface manipulating antimicrobial peptides. *J Extracell Biol*. 2023;2(3):e78. <https://doi.org/10.1002/jex2.78>
18. Tóth E, Turiák L, Visnovitz T, et al. Formation of a protein corona on the surface of extracellular vesicles in blood plasma. *J Extracell Vesicles*. 2021;10(11):e12140. <https://doi.org/10.1002/jev2.12140>
19. El Andaloussi S, Mäger I, Breakefield XO, Wood MJA. Extracellular vesicles: biology and emerging therapeutic opportunities. *Nat Rev Drug Discov*. 2013;12(5):347–357. <https://doi.org/10.1038/nrd3978>
20. Heidarzadeh M, Zarebkohan A, Rahbarghazi R, Sokullu E. Protein corona and exosomes: new challenges and prospects. *Cell Commun Signal*. 2023;21:1–15.
21. Welsh JA, Goberdhan DCI, O'Driscoll L, et al. Minimal information for studies of extracellular vesicles (MISEV2023): from basic to advanced approaches. *J Extracell Vesicles*. 2024;13(2):e12404. <https://doi.org/10.1002/jev2.12404>
22. Wu LNY, Genge BR, Dunkelberger DG, Legeros RZ, Concannon B, Wuthier RE. Physicochemical characterization of the nucleational core of matrix vesicles. *J Biol Chem*. 1997;272(7):4404–4411. <https://doi.org/10.1074/jbc.272.7.4404>
23. Hartree EF. Determination of protein: a modification of the Lowry method that gives a linear photometric response. *Anal Biochem*. 1972;48(2):422–427. [https://doi.org/10.1016/0003-2697\(72\)90094-2](https://doi.org/10.1016/0003-2697(72)90094-2)
24. Sebinelli HG, Borin IA, Ciancaglini P, Bolean M. Topographical and mechanical properties of liposome surfaces harboring Na,K-ATPase by means of atomic force microscopy. *Soft Matter*. 2019;15(13):2737–2745. <https://doi.org/10.1039/c9sm00040b>
25. Laemmli UK. Cleavage of structural proteins during the assembly of the head of bacteriophage T4. *Nature*. 1970;227(5259):680–685. <https://doi.org/10.1038/227680a0>
26. Ciancaglini P, Pizauro JM, Rezende AA, Rezende LA, Leone FA. Solubilization of membrane-bound matrix-induced alkaline phosphatase with polyoxyethylene 9-lauryl ether (polidocanol): purification and metalloenzyme properties. *Int J Biochem*. 1990;22(4):385–392. [https://doi.org/10.1016/0020-711X\(90\)90141-O](https://doi.org/10.1016/0020-711X(90)90141-O)
27. Andrilli LHS, Sebinelli HG, Favarin BZ, et al. NPP1 and TNAP hydrolyze ATP synergistically during biomineralization. *Purinergic Signal*. 2023;19(2):353–366. <https://doi.org/10.1007/s11302-022-09882-2>
28. Nogueira LFB, Cruz MAE, de Melo MT, et al. Collagen/κ-carrageenan-based scaffolds as biomimetic constructs for *in vitro* bone mineralization studies. *Biomacromolecules*. 2023;24(3):1258–1266. <https://doi.org/10.1021/acs.biomac.2c01313>
29. Moggridge S, Sorensen PH, Morin GB, Hughes CS. Extending the compatibility of the SP3 paramagnetic bead processing approach for proteomics. *J Proteome Res*. 2018;17(4):1730–1740. <https://doi.org/10.1021/acs.jproteome.7b00913>
30. Hughes CS, Foehr S, Garfield DA, Furlong EE, Steinmetz LM, Krijgsveld J. Ultrasensitive proteome analysis using paramagnetic bead technology. *Mol Syst Biol*. 2014;10(10):757. <https://doi.org/10.15252/msb.20145625>
31. Werner T, Sweetman G, Savitski MF, Mathieson T, Bantscheff M, Savitski MM. Ion coalescence of neutron encoded TMT 10-Plex reporter ions. *Anal Chem*. 2014;86(7):3594–3601. <https://doi.org/10.1021/ac500140s>
32. Franken H, Mathieson T, Childs D, et al. Thermal proteome profiling for unbiased identification of direct and indirect drug targets using multiplexed quantitative mass spectrometry. *Nat Protoc*. 2015;10(10):1567–1593. <https://doi.org/10.1038/nprot.2015.101>
33. Savitski MM, Wilhelm M, Hahne H, Kuster B, Bantscheff M. A scalable approach for protein false discovery rate estimation in large proteomic data sets. *Mol Cell Proteomics*. 2015;14(9):2394–2404. <https://doi.org/10.1074/mcp.M114.046995>
34. Kong AT, Leprevost FV, Avtonomov DM, Mellacheruvu D, Nesvizhskii AI. MSFragger: ultrafast and comprehensive peptide identification in mass spectrometry-based proteomics. *Nat Methods*. 2017;14(5):513–520. <https://doi.org/10.1038/nmeth.4256>
35. Ritchie ME, Phipson B, Wu D, et al. Limma powers differential expression analyses for RNA-seq and microarray studies. *Nucleic Acids Res*. 2015;43(7):e47. <https://doi.org/10.1093/nar/gkv007>
36. Huber W, von Heydebreck A, Sülthmann H, Poustka A, Vingron M. Variance stabilization applied to microarray data calibration and to the quantification of differential expression. *Bioinformatics*. 2002;18(suppl_1):S96–S104. https://doi.org/10.1093/bioinformatics/18.suppl_1.S96

37. Sauer GR, Wuthier RE. Fourier transform infrared characterization of mineral phases formed during induction of mineralization by collagenase-released matrix vesicles in vitro. *J Biol Chem*. 1988;263(27):13718–13724. [https://doi.org/10.1016/s0021-9258\(18\)68300-0](https://doi.org/10.1016/s0021-9258(18)68300-0)
38. Jiang S, Jin W, Wang YN, Pan H, Sun Z, Tang R. Effect of the aggregation state of amorphous calcium phosphate on hydroxyapatite nucleation kinetics. *RSC Adv*. 2017;7(41):25497–25503. <https://doi.org/10.1039/c7ra02208e>
39. Liam-Or R, Faruqi FN, Walters A, et al. Cellular uptake and in vivo distribution of mesenchymal-stem-cell-derived extracellular vesicles are protein corona dependent. *Nat Nanotechnol*. 2024;19(6):846–855. <https://doi.org/10.1038/s41565-023-01585-y>
40. Rilla K, Mustonen AM, Arasu UT, Härkönen K, Matilainen J, Nieminen P. Extracellular vesicles are integral and functional components of the extracellular matrix. *Matrix Biol*. 2019;75-76:201–219. <https://doi.org/10.1016/j.matbio.2017.10.003>
41. Bossi M, Hoylaerts MF, Millán JL. Modifications in a flexible surface loop modulate the isozyme-specific properties of mammalian alkaline phosphatases. *J Biol Chem*. 1993;268(34):25409–25416. [https://doi.org/10.1016/S0021-9258\(19\)74407-X](https://doi.org/10.1016/S0021-9258(19)74407-X)
42. Lopes HB, Freitas GP, Fantacini DMC, et al. Titanium with nanotopography induces osteoblast differentiation through regulation of integrin AV. *J Cell Biochem*. 2019;120(10):16723–16732. <https://doi.org/10.1002/jcb.28930>
43. Birk DE. Type V collagen: heterotypic type I/IV collagen interactions in the regulation of fibril assembly. *Micron*. 2001;32(3):223–237. [https://doi.org/10.1016/S0968-4328\(00\)00043-3](https://doi.org/10.1016/S0968-4328(00)00043-3)
44. Gordon MK, Hahn RA. Collagens. *Cell Tissue Res*. 2010;339(1):247–257. <https://doi.org/10.1007/s00441-009-0844-4>
45. Myllyharju J, Kivirikko KI. Collagens, modifying enzymes and their mutations in humans, flies and worms. *Trends Genet*. 2004;20(1):33–43. <https://doi.org/10.1016/j.tig.2003.11.004>
46. Leitingner B, Hohenester E. Mammalian collagen receptors. *Matrix Biol*. 2007;26(3):146–155. <https://doi.org/10.1016/j.matbio.2006.10.007>
47. Hicks D, Farsani GT, Laval S, et al. Mutations in the collagen XII gene define a new form of extracellular matrix-related myopathy. *Hum Mol Genet*. 2014;23(9):2353–2363. <https://doi.org/10.1093/hmg/ddt637>
48. Bateman A, Martin M-J, Orchard S, et al. UniProt: the universal protein knowledgebase in 2023. *Nucleic Acids Res*. 2023;51(D1):D523–D531. <https://doi.org/10.1093/nar/gkac1052>
49. Thouverey C, Malinowska A, Balcerzak M, et al. Proteomic characterization of biogenesis and functions of matrix vesicles released from mineralizing human osteoblast-like cells. *J Proteome*. 2011;74(7):1123–1134. <https://doi.org/10.1016/j.jpro.2011.04.005>
50. Chen X, Chen T, Xie H, Guo J. Salivary and serum levels of lactate dehydrogenase in oral submucous fibrosis: a meta-analysis. *Medicine*. 2024;103(15):e37788. <https://doi.org/10.1097/MD.00000000000037788>